Journal of Structural Engineering Vol.53A(March 2007) JSCE

Study on wind-induced instability of Super Long-Span Cable-Stayed Bridge

Pham Hoang KIEN *, Hitoshi YAMADA **, Hiroshi KATSUCHI *** and Eiichi SASAKI ****

* Graduate student, Dept. of Civil Eng., Yokohama National University, 79-7, Tokiwadai, Hodogaya-ku, Yokohama 240-8501
** Dr. of Eng., Professor, Dept. of Civil Eng., Yokohama National University, 79-7, Tokiwadai, Hodogaya-ku, Yokohama 240-8501
*** Dr. of Eng., Assoc. Prof., Dept. of Civil Eng., Yokohama Nat. University, 79-5, Tokiwadai, Hodogaya-ku, Yokohama 240-8501
**** Dr. of Eng., Assoc. Prof., Dept. of Civil Eng., Yokohama Nat. University, 79-7, Tokiwadai, Hodogaya-ku, Yokohama 240-8501

The static and dynamic wind-induced instability analyses of super long-span cable-stayed bridges with main span length of 1200～1800m are presented in this paper. Firstly, the static aeroelastic behaviors of bridges against displacement-dependent wind load are investigated by three-dimension geometrical nonlinear analysis. Secondly, the free vibration and flutter analyses are carried out. The comparisons of structural dynamic properties between cable-stayed and suspension bridges are discussed and the impact of the cable vibration effect on the dynamic characteristics and the flutter behavior is studied. The analytical results show that static instability controls the dimension of the girder and the safety against both static and dynamic instabilities can be ensured even with main span length of 1800m.

Key Words: cable-stayed bridge, long-span, lateral-torsion buckling, flutter

1. Introduction

Although "modern cable-stayed bridges" appeared only fifty years ago, however, continuous and rapid developments of material, structural form, structural details, analyses and construction methods have led the cable-stayed bridges to become very efficient. Economically, span limitation for application of cable-stayed bridges was said to be around 500m. However, currently two cable-stayed bridges with span exceeding 1000m are under construction and bridges with span of around 1200m have been investigated. The increase in span length of cable-stayed bridges has raised the concern not only about their overall elastic stability under in-plane load but also about wind-induced static and dynamic problems. With a self-anchored cable-stayed system, the girder will get no assistance from the cable system in carrying the lateral wind load. On the contrary, the girder will have to carry not only its own wind load but also half of the wind load on the stay cables. This implies that whereas the moment from lateral wind load on the girder will increase with the span raised to the second power, then the moment from wind on the stay cables will increase with the span raised to the third power. For this reason both the stresses and the deflections due to lateral wind load show a steep increase with the span length. For cable-stayed bridges with super long-span, wind load may cause lateral-torsion buckling or torsional divergence. With increasing span length, the aerodynamic instability, a phenomenon by which vibration amplitudes increase up to a collapse, raises its importance in design due to the decrease of natural frequencies. Therefore, another crucial factor might be this aerodynamic instability phenomenon.

In order to investigate the effect of increasing span lengths on aeroelastic stability and identify the possibility of long-span cable-stayed bridges, the main span lengths which varies from 1200～1800m are chosen as study parameter in this paper. By using four bridge models, aeroelastic stability analyses such as finite displacement analysis under displacement-dependent wind loads and flutter analysis under aerodynamic unsteady forces, which are very important issue in the design of super long-span cable-stayed bridges, are carried out. Finally, the possibility and limitations of long-span cable-stayed bridges are discussed.

The self-anchored system is used in the present study. In order to reduce the compressive axial force in the girder, the partially earth-anchored system has been proposed. It is also expected that this system can reduce the deflection and stress resultants of the girder under wind load. From the study carried out by Nagai (1996), by using a 1400m cable-stayed bridge model, the deflection and stress resultants were found around 10% smaller than those of self-anchored system. However, critical wind speed of both systems under displacement-dependent wind load was nearly the same. Another proposal made by Dischinger is the combined system of suspension and cable-stayed systems. To extend the span using this system, the span limitation of the self-anchored system plays an important role. Hence, the identification of the span limitation of the self-anchored system is of major importance.

2. Bridge models

The general configurations of four studied models with main span length of 1200m, 1400m, 1600m and 1800m, are shown in Fig.1～4. In order to consider the balance of vertical load (gravity load) acting on towers, side span length is assumed to be nearly half of the main span length. Intermediate piers are installed at a distance of 100 meters from bridge ends in order to increase in-plane flexural rigidity of the bridge. Multi-stays system of semi-fan arrangement and two inclined planes of cables are employed. The cables are anchored at distances of 20m at the girder and of 4m at the tower. Fig.1(b),(c)～4(b),(c) show the front view and cross section of the tower. The tower height from the deck level is one fifth of the main span length. A-shaped tower is chosen because it is the optimal solution not only for appearance but also for wind stability, especially for super long-span cable-stayed bridges.

Fig.5 shows the cross-sectional shape of the girder. For cable-stayed bridges with spans of medium length and relatively wide girders, it will generally be unnecessary to streamline the girder as aerodynamic stability can be achieved even with bluff cross sections. However, when moving into the range of long-span bridges, the streamlined box girder will be required. In this study, the streamlined box girder with relatively small dimensions (horizontal slenderness ratio of span/width =55 and vertical slenderness ratio of span/depth =400) is selected. The above slenderness ratios presently are thought as limitation with respect to the structural stability. Horizontal slenderness ratio of span/width is an important parameter when investigating wind-induced instability of long-span cable-stayed bridges. In researches carried out by Nagai (1998), the span/width ratio was chosen as study parameter and minimum girder width ensuring safety against static and dynamic instabilities under wind load was investigated. It was found that, from the viewpoint on steel volume, the cross-sectional shape with the span/width ratio of around 55 will give the most economical value.

The prestresses of the cables are computed by assuming that the vertical component of the prestress of any cable is equal to the dead load reaction obtained by supposing that the bridge deck is rigidly supported at the cable-deck intersections. Cross-sectional area of the cables is determined under the condition that the ratio of live to dead loads is 0.25 and the allowable stress is 588MN/m^2. Dimension of the girder is verified by using the following criteria.

$$\sigma_D + \sigma_L < \sigma_y / \nu_1 \qquad (\nu_1 = 1.7) \tag{1}$$

$$\sigma_D + \sigma_W < \sigma_y / \nu_2 \qquad (\nu_2 = 1.7/1.5 = 1.13) \tag{2}$$

where, σ_D, σ_L and σ_W are the normal stresses from dead, live and wind loads, respectively and ν is the factor of safety.

When calculating the wind-induced stress, the design wind speed at the height of 10 meters U_{10} is assumed to be 60m/s. The drag coefficients of towers and cables are assumed to be 1.2 and 0.7, respectively. To satisfy the criterion defined in Eq.(2), thickness of plate is increased as shown in Fig.5(b) in order to efficiently increase out-of-plane flexural rigidity of the girder. In Fig.1(a)～4(a), X_u is the region where thickness of plate is increased.

The material grade SM570 with yield point (σ_y) of 451MN/m^2 is used for both girder and towers. The dimensions of girder cross section and cross-sectional properties of the tower and girder are shown in Table 1, 2 and 3, respectively. In the Table 3, the figures in the parenthesis are for the reinforced girder.

The dead load intensity of girder (W_G) and tower (W_T) is calculated by using the following equations:

$$W_G = 1.4 A_G \gamma_s + 70.0 \tag{3}$$

$$W_T = 1.4 A_T \gamma_s \tag{4}$$

where, A_G and A_T are the steel cross-sectional area (m^2) per unit length of the girder and tower, which resist the axial force, 1.4 is the coefficient accounting for weight of steel members such as diaphragms, cross-frames and so on, γ_s is the weight density of steel (78.5KN / m^3), 70.0 (KN / m) is the suggested value for the superimpose dead load.

Table 1 Dimensions of girder cross section

Model	1200m	1400m	1600m	1800m
Width (m)	22	26	30	33
Depth (m)	3.0	3.5	4.0	4.5

Table 2 Cross-sectional properties of the tower

Model	A_T(m^2)	I_x(m^4)	I_y(m^4)	J (m^4)
1200m	2.16	24.32	34.0	42.67
1400m	2.64	46.0	60.48	78.55
1600m	3.12	77.76	98.0	130.3
1800m	3.60	121.5	148.5	200.7

Table 3 Cross-sectional properties of the girder

Model	A_G(m^2)	I_x(m^4)	I_y(m^4)	J (m^4)	X_u(m)
1200m	1.03 (1.56)	1.54 (2.60)	49.84 (92.59)	3.76 (5.38)	20
1400m	1.20 (1.92)	2.44 (3.95)	78.20 (165.0)	6.13 (9.40)	60
1600m	1.43 (2.21)	3.74 (5.45)	120.3 (249.4)	8.37 (11.1)	100
1800m	1.54 (2.37)	5.05 (6.99)	154.6 (325.2)	11.9 (15.4)	160

figures in ( ) : for the reinforced girder

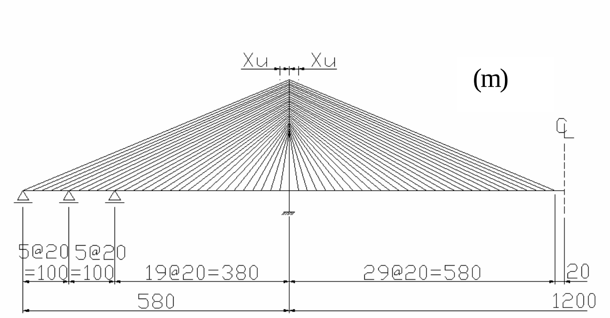

(a) Side-view

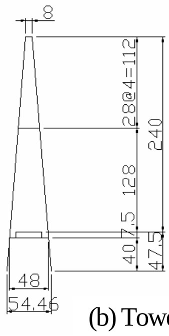

(b) Tower

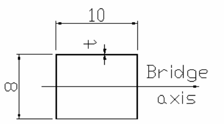

(c) Cross section of tower

Fig.1 1200m model

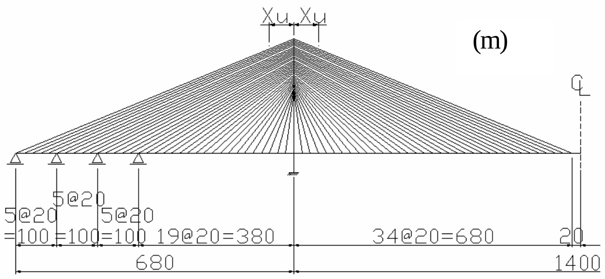

(a) Side-view

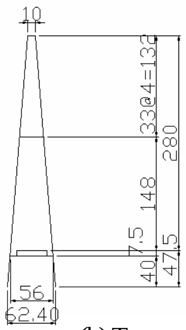

(b) Tower

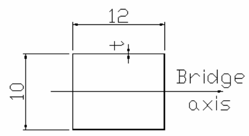

(c) Cross section of tower

Fig.2 1400m model

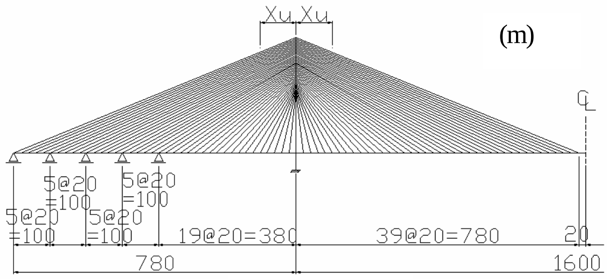

(a) Side-view

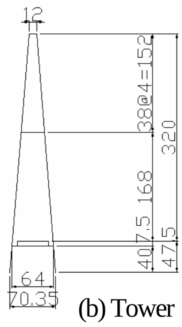

(b) Tower

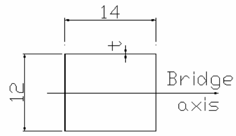

(c) Cross section of tower

Fig.3 1600m model

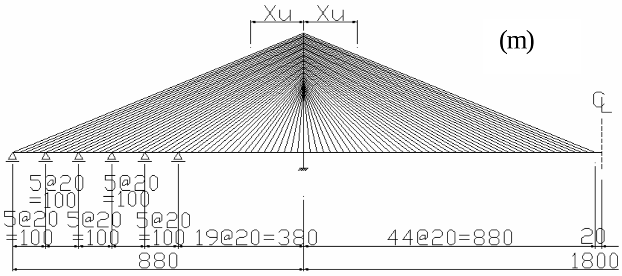

(a) Side-view

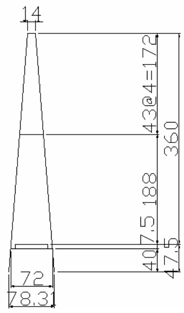

(b) Tower

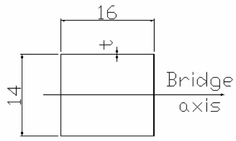

(c) Cross section of tower

Fig.4 1800m model

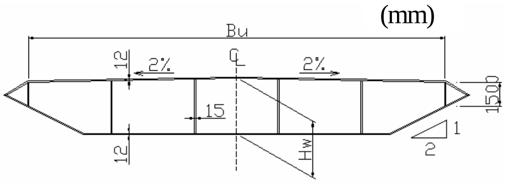

(a) Basic cross section

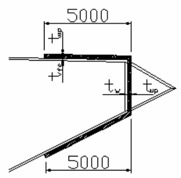

model	1200m	1400m	1600m	1800m
t_{up}(mm)	24	30	32	34

(b) Increase of plate thickness

Fig.5 Cross section of the girder

3. Lateral-torsion buckling analysis

3.1 Modeling of displacement-dependent wind loads

A 3D large displacement analysis is carried out by considering the wind loads acting on the girder, towers and cables simultaneously (Fig.6).

Three components of the wind load on the deformed girder are displacement-dependent and can be written as follows,

$$\begin{aligned} D(\alpha) &= 0.5\rho U_Z{}^2 A_n C_D(\alpha) \\ L(\alpha) &= 0.5\rho U_Z{}^2 B C_L(\alpha) \\ M(\alpha) &= 0.5\rho U_Z{}^2 B^2 C_M(\alpha) \end{aligned} \qquad (5)$$

where, $D(\alpha)$, $L(\alpha)$ and $M(\alpha)$ are, respectively, the drag force, lift force, and aerodynamic moment per unit span, U_z is the design wind speed, ρ is the air density, A_n is the vertical projection of the girder, B is the total width of the girder, C_D, C_L and C_M are aerodynamic coefficients and α is the angle attack of the wind. Generally, aerodynamic coefficients vary depending on the value of ratio B/D (B and D are, respectively, the width and depth of the girder). However, in the range of small angle attack, the dependency of aerodynamic coefficients on the above ratio is not so remarkable. Therefore in this study, regarding to aerodynamic coefficients, the values obtained from wind tunnel test of the Meiko cable-stayed bridge, for which a similar streamlined box girder has been employed, are used (Fig .7).

The wind loads acting on towers and cables are considered as distributed drag force and given as follows

$$\begin{aligned} &\text{towers}: \quad D = 0.5\rho U_z^2 A C_D \quad C_D = 1.2 \\ &\text{cables}: \quad D = 0.5\rho U_z^2 d C_D \quad C_D = 0.7 \end{aligned} \qquad (6)$$

where, A is the width of the tower in bridge axis direction and d is the cables diameter.

The design wind speed U_z at the height of z is given by

$$U_Z = (z/10)^{1/7} U_{10} \qquad (7)$$

where, U_{10} is the wind speed at the height of 10 meters.

When the girder is subjected to the wind load, it not only displaces in the horizontal and vertical direction, but also rotates. Since aerodynamic coefficients are expressed as a function of the angle of attack, the wind loads vary due to the rotation of the girder. Under the action of wind load and girder rotation, it will also result in the change of the tension in cables and its acting direction. Furthermore, if the span exceeds 1000 meters, it is known that the wind load from the cables becomes larger than that acting on the girder directly. Hence, for correctly identifying static instability under wind load, it is necessary to take all the above phenomena into account and calculate the convergence value by repetition calculation.

The Euclidean norm of the aerodynamic coefficients of lift, drag and pitch moment is taken as convergence criterion, which can be expressed as

$$\left\{ \frac{\sum_1^{Na}\left[C_K(\alpha_j) - C_K(\alpha_{j-1})\right]^2}{\sum_1^{Na}\left[C_K(\alpha_{j-1})\right]^2} \right\}^{1/2} \le \varepsilon_K \quad (K = L, D, M) \qquad (8)$$

where, ε_K is the convergence accuracy and N_a is the total number of the nodes applied with wind loads.

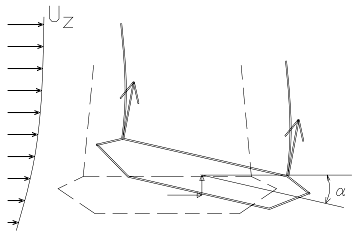

Fig.6 Motion of the girder and cables

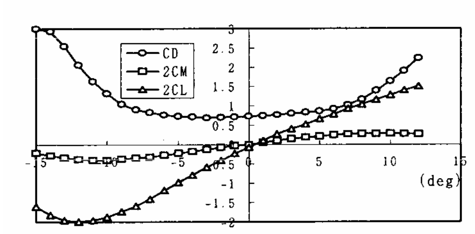

Fig.7 Aerodynamic coefficients

3.2 Results and Discussions

Fig.8 shows the horizontal and vertical displacements as well as the rotational angle at the middle of the center span. Although the horizontal displacements increase with the increasing of span lengths, however, in span range of 1200～1800m horizontally unstable phenomenon is not seen even with the wind speed up to 80m/s (Fig.8 (a)). In the range of low wind speed the vertical displacements and rotational angle are small, but at speed exceeding the design wind speed their nonlinear behavior becomes prominent and they will diverge when wind speed reaches at a certain value as shown in the Fig.8 (b), (c). This unstable phenomenon, in which torsional and vertical displacements increase rapidly, is defined as lateral-torsion buckling. The wind speed, for which the convergence criterion Eq.(8) could not be satisfied, is considered as static critical wind speed. From these analytical results, it can be concluded that when examining the static wind-resistant characteristics of a long-span cable-stayed bridge, it is necessary to pay attention not only to the out-of-plane response but also to the entire behavior of the structure.

Although the critical wind speed decreases with the increase of span lengths, there are no change in the static wind-resistant characteristics when span lengths vary in the range of 1200～1800m. Furthermore, for all studied models, the calculated critical wind speeds are high enough compared with the design wind speed defined in this paper. In other words, it can be realized that in the usual design wind speed range, all studied models possess sufficient static wind-resistant stability.

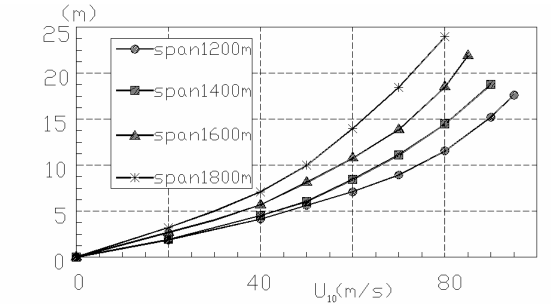

(a) Horizontal displacement

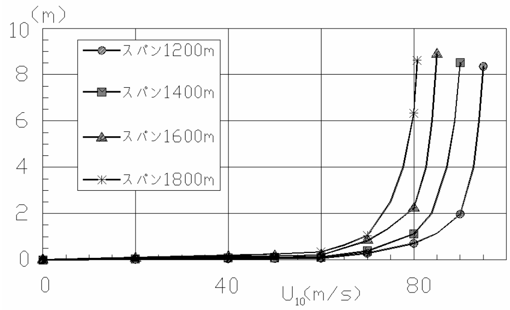

(b) Vertical displacement

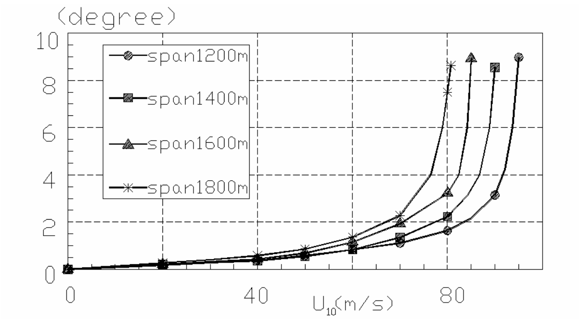

(c) Rotational angle

Fig.8 Displacements at the middle of center span

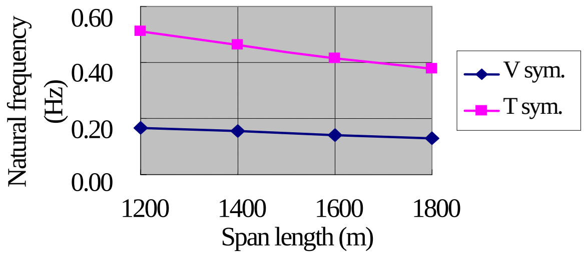

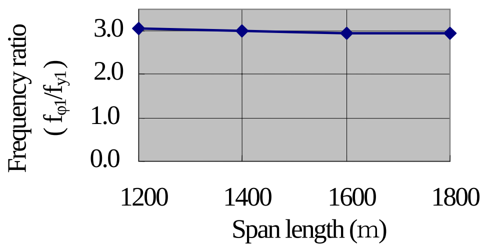

Fig.9 Frequency decrement due to span length

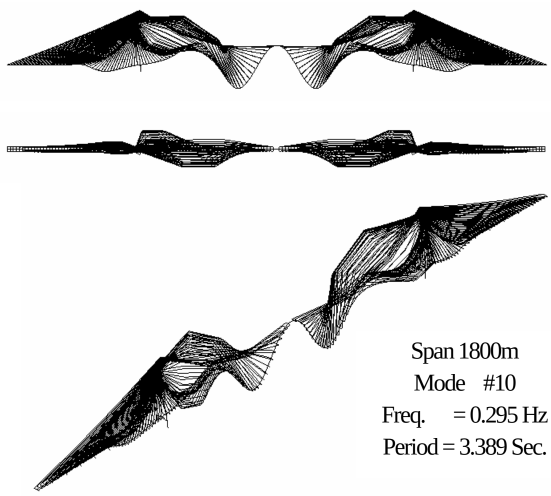

Fig.10 Free vibration mode shape

4. Free vibration and Flutter Analysis

4.1 Dynamic characteristics of the free vibration

As shown in Fig. 9, although the natural frequencies, the most basic dynamic characteristic, decrease with increasing span length, however, both torsional and bending frequencies show similar decrement tendency and the ratio of torsional frequency to vertical bending frequency decreases little regardless of the span length. It is found that there are no sudden changes in the dynamic characteristics of cable-stayed bridges even with main span length varying in the range of 1200～1800m. Fig. 10 shows an example of mode shape of the free vibration when the vibration characteristics of stay cables are taken into consideration. Such vibrations, which are usually overlooked in analysis, in addition to being complex, are strongly coupled with the bridge deck and tower motions. This effect requires multi-element cable discretization and can not be predicted using a one-element cable discretization system. To investigate the effects of cable vibrations on the dynamic behaviors of cable-stayed bridges, an approach using modal co-ordinate in cables to reduce the freedom of cable has been developed by Nagai (1992). However, there is another convenient approach of using the multi-element model, which discretizes each stay cable into several elements. The latter is adopted in this study.

Table 4 shows the comparison of dynamic characteristics between suspension and cable-stayed bridges (with streamlined box girder) and flutter wind speed calculated by Selberg's formula. Although the mass is approximately same in the case of a cable-stayed bridge and a suspension bridge, however the bending frequency of the cable-stayed bridge is higher as the stay-cables contribute greatly to vertical rigidity, while the polar moment of inertia is smaller than that in the suspension bridge. Furthermore, with combination of A-shaped tower and two stay-cable planes, which are used in this paper, the cable-stayed bridges obtain high torsional rigidity compared with the suspension bridges and as a result, the torsional frequency is higher than that in the suspension bridges. The flutter wind speed of cable-stayed bridge is higher and it is found that cable-stayed bridge has more favorable dynamic wind stability.

Table 4 Comparison of dynamic characteristics

	Bridge	Span (m)	Mass (t/m/br)	Polar moment of inertia (tm^2/m/br)	Natural frequency (symm.) (Hz)		Flutter speed (m/s)
					Bending	Torsion	
Susp-ension bridge	Kurushima No.2	1020	22.27	2394	0.149	0.361	95
	Kurushima No.3	1030	22.10	2359	0.155	0.361	94
	Great Belt East	1624	22.74	2470	0.099	0.272	75
Cable-stayed bridge	Tatara	890	20.06	1089	0.199	0.569	140
	Model 1	1200	19.55	813	0.168	0.512	119
	Model 2	1400	21.68	1295	0.154	0.462	114
	Model 3	1600	24.75	2061	0.141	0.416	111
	Model 4	1800	26.35	2719	0.128	0.378	105

4.2 Flutter instability analysis

In this study, mode superposition method is used for 3-D FEM flutter analysis. The equations of motion of the whole structure under wind action can be written as

$$\mathrm{M}\ddot{\mathrm{u}}+\mathrm{C}\dot{\mathrm{u}}+\mathrm{K}\mathrm{u}=\mathrm{F}_D\mathrm{u}+\mathrm{F}_U\dot{\mathrm{u}}+\mathrm{F}_A\ddot{\mathrm{u}} \quad (9)$$

$$\mathrm{u}=[u_g, f_g, v_g, u_c, v_c]^T \quad (10)$$

where, **u** : displacement vector, **M** : mass matrix, **C** : structural damping matrix, **K** : stiffness matrix, $\mathbf{F}_D$, $\mathbf{F}_U$ and $\mathbf{F}_A$: displacement proportional expression, velocity proportional expression and acceleration proportional expression of motion-dependent aerodynamic force coefficient matrix, respectively. Assuming the harmonic vibration, relationships between displacement, velocity and acceleration can be expressed as

$$\mathrm{u}=-\frac{1}{\omega^2}\ddot{\mathrm{u}}, \quad \dot{\mathrm{u}}=-\frac{i}{\omega}\ddot{\mathrm{u}}, \quad k=\frac{\omega b}{U} \quad (11)$$

where ω, U and k are natural circular frequency, wind speed and reduced frequency, respectively.

Substituting Eq.(11) to Eq.(9), the equations of motion become a complex eigenvalue problem as

$$(\mathrm{M}-\mathrm{F})\ddot{\mathrm{u}}+\mathrm{K}\mathrm{u}=0 \quad (12)$$

$$\mathrm{F}_D\mathrm{u}+\mathrm{F}_U\dot{\mathrm{u}}+\mathrm{F}_A\ddot{\mathrm{u}}=\mathrm{F}\ddot{\mathrm{u}} \quad (13)$$

Complex eigenvalue analysis is carried out by assuming the reduced frequency and using mode superposition method. Solving Eq.(12), we obtain n-sets of complex frequencies $\omega=\omega_R+i\omega_I$ and complex vibration modes $\boldsymbol{\Phi}=\boldsymbol{\Phi}_R+i\boldsymbol{\Phi}_I$ under wind action for each assumed reduced frequency k. Then we can see the stability of the structure by δ_m which indicates the logarithmic damping of the m-th mode as

$$\delta_m=\omega_{mI}\Big/\sqrt{\omega_{mR}^2+\omega_{mI}^2} \quad (14)$$

where, ω_{mR} and ω_{mI} are real-part and imaginary-part of the m-th complex circular frequency under wind action, respectively.

In this study, the unsteady lift force and aerodynamic moment of the girder are derived based on flat plate theory and are given by

$$\downarrow\ L_g=-\pi\rho b^2\left(\ddot{u}_g+U\dot{\phi}_g\right)-2\pi\rho UbC(k)\left(\dot{u}_g+U\phi_g+\frac{b}{2}\dot{\phi}_g\right) \quad (15)$$

$$\curvearrowright\ M_g=\pi\rho b^3\left(-\frac{U}{2}\dot{\phi}_g-\frac{b}{8}\ddot{\phi}_g\right)+2\pi\rho Ub^2\cdot\frac{1}{2}C(k)\left(\dot{u}_g+U\phi_g+\frac{b}{2}\dot{\phi}_g\right) \quad (16)$$

where, $C(k)$ and ρ are the Theodorsen function and the air density, respectively.

The unsteady drag force of the girder and the unsteady drag and lift forces of the cable are derived based on quasi-steady theory and are given by

$$\rightarrow\ P_g=-\rho hC_{Dg}U\dot{v}_g \quad (17)$$

$$\rightarrow\ P_c=-\rho dC_{DC}U\dot{v}_C \quad (18)$$

$$\downarrow\ L_c=-\left(\frac{1}{2}\right)\rho dC_{DC}U\dot{u}_C \quad (19)$$

where h, d, C_{Dg} and C_{DC} are the vertical projection of the girder, cable diameter, drag coefficient of the girder and cable, respectively.

According to Eq.(15) ～ Eq.(19), motion-dependent aerodynamic force coefficient matrices can be rewritten as

$$\mathrm{F_D} = 2\pi\rho U^2 b\left[\begin{array}{cc:c} 0 & -C(k) & \\ 0 & (b/2)C(k) & 0 \\ \hdashline \multicolumn{2}{c:}{0} & 0 \end{array}\right] \tag{20}$$

$$\mathrm{F_U} = \rho U\left[\begin{array}{cc:ccc} -2\pi bC(k) & -\pi b^2\{1+C(k)\} & \multicolumn{3}{c}{\multirow{2}{*}{0}} \\ \pi b^2 C(k) & -\pi b^3\{1-C(k)\}/2 & & & \\ \hdashline \multicolumn{2}{c:}{\multirow{3}{*}{0}} & -hC_{Dg} & & \\ & & & -dC_{DC}/2 & \\ & & & & -dC_{DC} \end{array}\right] \tag{21}$$

$$\mathrm{F_A} = \pi\rho b^2\left[\begin{array}{cc:c} -1 & 0 & \\ 0 & -b^2/8 & 0 \\ \hdashline \multicolumn{2}{c:}{0} & 0 \end{array}\right] \tag{22}$$

$$\mathrm{F} = \left[\begin{array}{cc:ccc} -\pi\rho b^2 L_u & -\pi\rho b^3 L_\phi & \multicolumn{3}{c}{\multirow{2}{*}{0}} \\ -\pi\rho b^3 M_u & -\pi\rho b^4 M_\phi & & & \\ \hdashline \multicolumn{2}{c:}{\multirow{3}{*}{0}} & \rho bhiC_{Dg}/k & & \\ & & & \rho bdiC_{DC}/(2k) & \\ & & & & \rho bdiC_{DC}/k \end{array}\right] \tag{23}$$

Table 5 Flutter instability analysis

Span (m)	Selberg's formula	Flutter onset wind speed (m/s)				
		One-element cable discretization	Multi-element cable discretization		Wind speed increment	
			Without accounting for cable unsteady force	Accounting for cable unsteady force	Due to cable discretization	Due to cable unsteady force
1200	118.6	109.4	111.8	119.1	2.4	7.3
1400	113.5	103.6	105.6	114.8	2.0	9.2
1600	111.2	97.9	99.6	111.3	1.7	11.7
1800	105.3	92.8	94.4	113.1	1.6	18.7

Table 5 shows flutter onset wind speeds obtained by Selberg's formula and by flutter analysis. In order to investigate the effects of transverse vibration of cables on dynamic behaviors of the structure, the flutter analysis is carried out with and without accounting for cable transverse vibration modes.

For all studied models, flutter onset wind speeds are higher than static instability wind speed. Furthermore, higher flutter wind speed will be obtained when cable transverse vibrations were taken into consideration. When accounting for cable vibrations, the aerodynamic damping forces of the cables are obtained due to the coupling between cable vibrations and bridge deck, tower motions, and this damping force will shift upward the flutter wind speed. The effect of cable vibrations increase with increasing span length and it is found that this effect is significant in the case of cable-stayed bridge with super long-span. There is relatively good agreement between the results of multi-mode flutter analysis and flutter wind speeds calculated by Selberg's formula, however evaluation by Selberg's formula will result in slightly higher wind speed. This is caused due to the coupling characteristics of torsional mode shapes. When investigating the first torsional mode, coupling of this mode with lateral bending motion was found. Therefore, a large equivalent polar moment of inertia is calculated and when evaluated by Selberg's formula, which deals with only first vertical bending and first torsional mode, a higher wind speed will be obtained.

5. Concluding remarks

It is believed by many engineers that the suspension system is an unique economical solution when span length exceeds 1000m. In researches carried out by Nagai (1998), it is reported that span limitation for application of self-anchored cable-stayed system is around 1400m. In this paper, the span length exceeding 1400m also is taken into object of research. Using four bridge models with span length varying from 1200～

1800m, lateral-torsion buckling analysis under displacement-dependent wind loads and flutter analysis under aerodynamic unsteady forces, which are very important issue in the design of super long-span cable-stayed bridges, are carried out. Main results obtained from this study are summarized as follows.

1) There are no sudden changes in the both static and dynamic wind-resistant characteristics of cable-stayed bridge even with main span length varying in the range of 1200～1800m.
2) Under static wind load, horizontally unstable phenomenon is not found. Lateral-torsion buckling occurs at a certain critical wind speed. For all four studied models, critical wind speeds are higher than the design wind speed.
3) Due to the inherent stiffness of the cable system, cable-stayed bridges show off a priori 1.5 - 2.0 times higher dominant eigenfrequencies than suspension bridges and are, hence, less sensitive against flutter instability. A further stabilizing effect can be activated by using A-shaped tower and two stay-cable planes, which are used in this study to shift upward the torsional eigenfrequency so that a high eigenfrequency ratio occurs.
4) Higher flutter wind speed will be obtained when cable transverse vibrations were taken into consideration. This is due to the effect of aerodynamic damping forces of the cables, which are obtained by the coupling between cable vibrations and bridge deck, tower motions. The effect of cable vibrations increase with increasing span length and will be significant in the case of super long-span cable-stayed bridge.
5) Flutter onset wind speeds are higher than static instability wind speeds. Static instability controls the dimension of girder.
6) Although the girder has relatively small dimensions with horizontal slenderness ratio of span/width =55 and vertical slenderness ratio of span/depth =400, safety against both static and dynamic aeroelastic instabilities is ensured. Slenderness ratios used in this paper are higher compared with those used in the conventional design. If the girder near the tower was reinforced appropriately, it is expected to use the girder cross section with considerably small size.
7) It is expected, depending on the soil condition at the construction site, that the self-anchored cable-stayed bridge is a powerful alternative, even with span length of around 1800m.

References

1) Boonyapinyo, V. : Nonlinear Static Instability Analysis of Long-Span Cable-Stayed Bridges under Gravity and Wind Loads, Doctoral Thesis, Yokohama National University, 1993.
2) Endo, T., Iijima, T., Okukawa, A. and Ito, M. : The technical challenge of a long cable-stayed bridge – Tatara Bridge, *Proceedings of CABLE-STAYED BRIDGES Recent Development and their Future*, Yokohama, Japan, 1991.
3) Endo, T. : Some studies on structural planning of long-span cable-stayed bridge, *Journal of Structural Mechanics and Earthquake Engineering*, JSCE, No. 567/I-35, pp.171-188, 1997.
4) Honshu-Shikoku Bridge Authority : *Annual Rept. Technical Comm. Wind Resistant Design of Honshu-Shikoku Bridges*, Japan, 1990.
5) Hoshino, M. and Miyata, T. : Design Trial of A Long-span Cable-stayed Bridge with Center Span Length of 1000m, *Bridge and Foundation Eng*, 90-2, pp.15-22, 1990 (in Japanese)
6) Nagai, M., Asano, K., Kishimoto, S. and Mizukami, Y. : Feasible cross-sectional shapes of the girder in long-span self-anchored cable-stayed bridges, *Journal of Structural Engineering*, JSCE, Vol. 39A, pp.1075-1088, 1993 (in Japanese).
7) Nagai, M., Ishida, T., Xie, X., Yamaguchi, H. and Fujino, Y. : Minimum girder width ensuring safety against static and dynamic instabilities of long-span cable-stayed bridges under wind load, *Journal of Structural Engineering*, JSCE, Vol. 44A, pp.1191-1198, 1998 (in Japanese).
8) Nagai, M., Xie, X., Yamaguchi, H. and Nogami, K. : Effect of girder depth on ultimate strength of multi-cable type cable-stayed bridges, *Journal of Structural Engineering*, JSCE, Vol. 45A, pp.77-82, 1999 (in Japanese).
9) Nogami, K., Iwasaki, H., Narita, N. and Nagai, M. : Stability check of super long-span cable-stayed bridges, *Journal of Structural Engineering*, JSCE, Vol. 45A, pp.83-92, 1999 (in Japanese).
10) Xie, X., Nagai, M., Yamaguchi, H. and Ito, M. : Static behaviors of self-anchored and partially earth-anchored cable-stayed bridges under wind load, *Journal of Structural Engineering*, JSCE, Vol. 42A, pp.1005-1012, 1996 (in Japanese).
11) Xie, X., Yamaguchi, H. and Nagai, M. : Effect of girder width on static instability of long-span cable-stayed bridges, *Journal of Structural Engineering*, JSCE, Vol. 43A, pp.1221-1228, 1997 (in Japanese).
12) Miyata, T. : Design consideration for wind effects on long cable-stayed bridges, *Proceedings of CABLE-STAYED BRIDGES Recent Development and their Future*, Yokohama, Japan, 1991.

(Received September 11, 2006)